

1 Supplementary Materials for:

2 **Cloud condensation nuclei (CCN) and HR-ToF-AMS measurements at a coastal site in**
3 **Hong Kong: Size-resolved CCN activity and closure analysis**

4 J.W. Meng¹, M.C. Yeung², Y.J. Li¹, B.Y.L. Lee¹, C.K. Chan^{1,2,*}

5 ¹Division of Environment, Hong Kong University of Science and Technology, Clear Water Bay,
6 Hong Kong SAR, China

7 ²Department of Chemical and Biomolecular Engineering, The Hong Kong University of
8 Science and Technology Clear Water Bay, Hong Kong SAR, China

9 *Correspondence to: C.K. Chan (keckchan@ust.hk)

10

11

12

13

14

15

16

17

18

19

20

21

22

23

24

25

26

27 **1 Uncertainty of N_{CN} , N_{CCN} , κ_{CCN} and κ_{AMS}**

28 The relative uncertainty of N_{CN} (ε_{CN}) is mainly determined by the uncertainty in the flow
29 rate (10%) and number counting (10%) of TSI 3785 WCPC, and the overall ε_{CN} is 14%. The
30 relative N_{CCN} (ε_{CCN}) uncertainty depends on the concentration-dependent Poisson statistical
31 uncertainty and the CCNc flow rate uncertainty (Moore et al., 2012; Roberts and Nenes, 2005):

$$32 \quad \varepsilon_{\text{CCN}}^2 = \varepsilon_{Q_{\text{CCN}}}^2 + \frac{\tau_{\text{CCN}}}{N_{\text{CCN}}Q_{\text{CCN}}} \quad (1)$$

33 where τ_{CCN} is the integration time (1 second) of CCNc optical particle counter (OPC) and Q_{CCN}
34 is the sample flow rate of CCNc ($45 \text{ cm}^3 \text{ min}^{-1}$), the $\varepsilon_{Q_{\text{CCN}}}$ is about 5%. Overall, ε_{CCN} increases
35 with the decrease of SS , since the N_{CCN} decreases as SS decreases. The maximum uncertainty is
36 $\sim 38\%$ at $SS = 0.15\%$ in this study.

37 The uncertainty of κ_{CCN} comes from the accuracy of the dry particles classified by the DMA
38 and the uncertainty of the activation efficiency ($\varepsilon_{\text{CCN}/\text{CN}}$) used for D_{50} determination. The
39 $\varepsilon_{\text{CCN}/\text{CN}}$ can be obtained from

$$40 \quad \varepsilon_{\text{CCN}/\text{CN}}^2 = \varepsilon_{\text{CN}}^2 + \varepsilon_{\text{CCN}}^2 \quad (2)$$

41 The sizing accuracy of DMA was determined by the accuracy of DMA sheath flow rate and
42 classifying voltage. The typical value is less than 3% (Wang et al. 2003). The overall uncertainty
43 in derived κ_{CCN} ranges from 23% to 39%.

44 The uncertainty of κ_{AMS} comes from the uncertainty in κ_{CCN} (as κ_{org} and κ_{inorg} are derived
45 from κ_{CCN} shown in main text), as well as the species densities and the volume fractions of
46 organics and inorganics that are derived from the AMS mass concentrations. The uncertainty of
47 inorganic compositions densities could be considered negligible. For organics, a mean value of
48 1.36 ± 0.11 for H:C and 0.40 ± 0.11 for O:C were found (Lee et al., 2013), and the organic
49 density estimated from the ratio of O:C ranging from 0.29 to 0.46 and H:C ranging from 1.49 to
50 1.28 were from 1.15 g cm^{-3} to 1.35 g cm^{-3} (Kuwata et al., 2011). The uncertainty of an assumed
51 organic density of 1.3 g cm^{-3} is less than 8%, which is smaller than the uncertainty in mass
52 concentrations ($\sim 30\%$) measured by AMS because of the uncertainty in collection efficiency

53 (*CE*) (Middlebrook et al., 2012). The large fractions of semi-volatile oxygenated organics
54 aerosols (SV-OOA) (23.5%) and low-volatile oxygenated organic aerosols (LV-OOA) (53.9%)
55 suggested that particles were largely aged and likely internally mixed. An internal mixing state
56 implies that the influences of *CE* on both NR inorganic and organic species are in the same
57 degree, thus have little impact on the derived volume fractions. In all, an uncertainty of 16% is
58 estimated for determination of inorganics and organics volume fractions, which are mainly due
59 to the uncertainties in relative ionization efficiency (*RIE*) (Bahreini et al., 2009; Mei et al.,
60 2013). However, it is worth noting that the low signal-to-noise ratios of AMS measurements for
61 small particles ($D_m < 50$ nm) will make the derived κ_{AMS} less reliable.

62

63

64 2 Supporting Figures

65

66

67

68

69

70

71

72

73

74

75

76

77

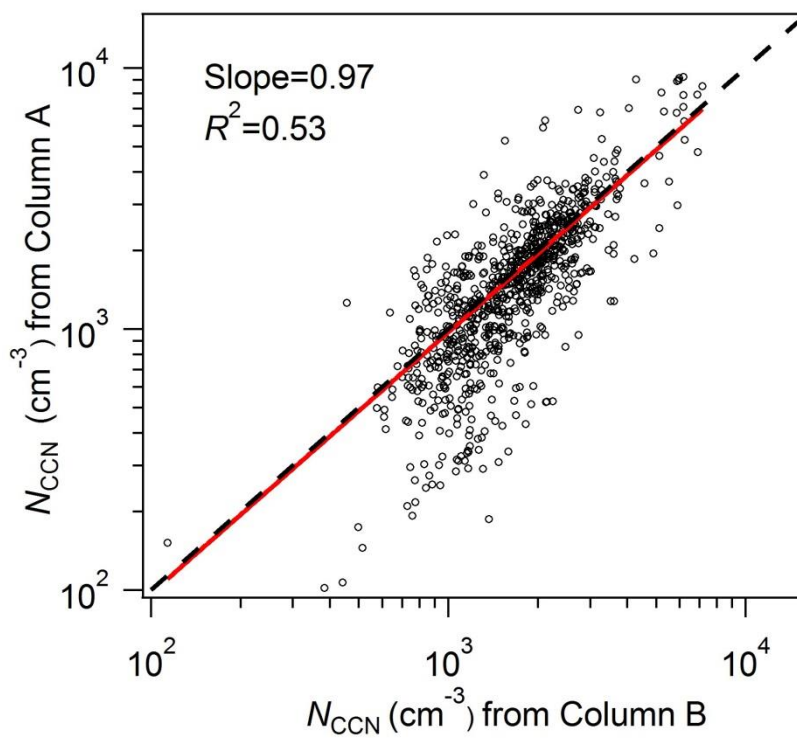
78

79

80

81

82



83 Fig.S1 Correlation of N_{CCN} from size-resolved CCN measurement (Column A) and bulk
84 measurement (Column B).

85
86
87
88
89
90
91
92
93
94
95
96
97
98
99
100
101
102
103
104

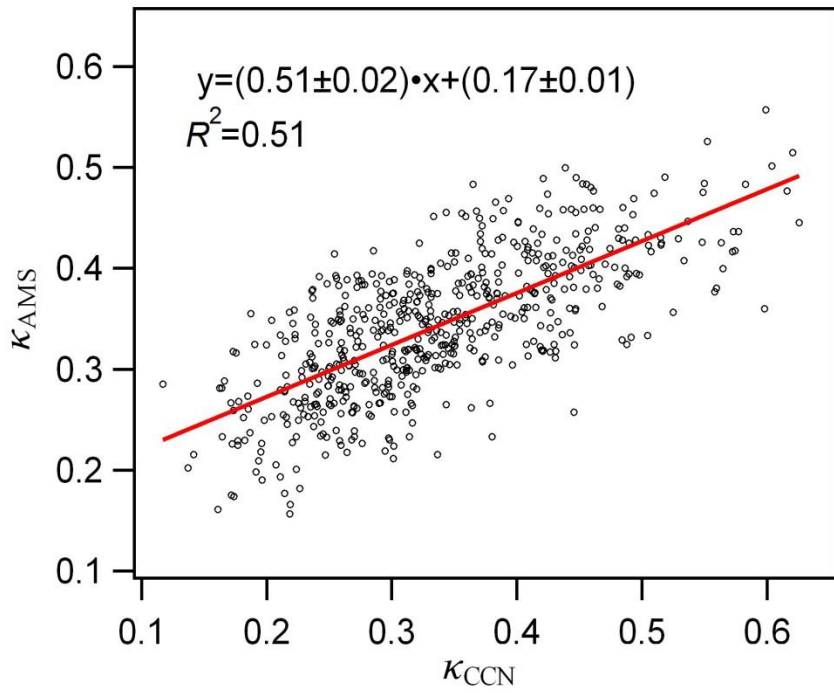
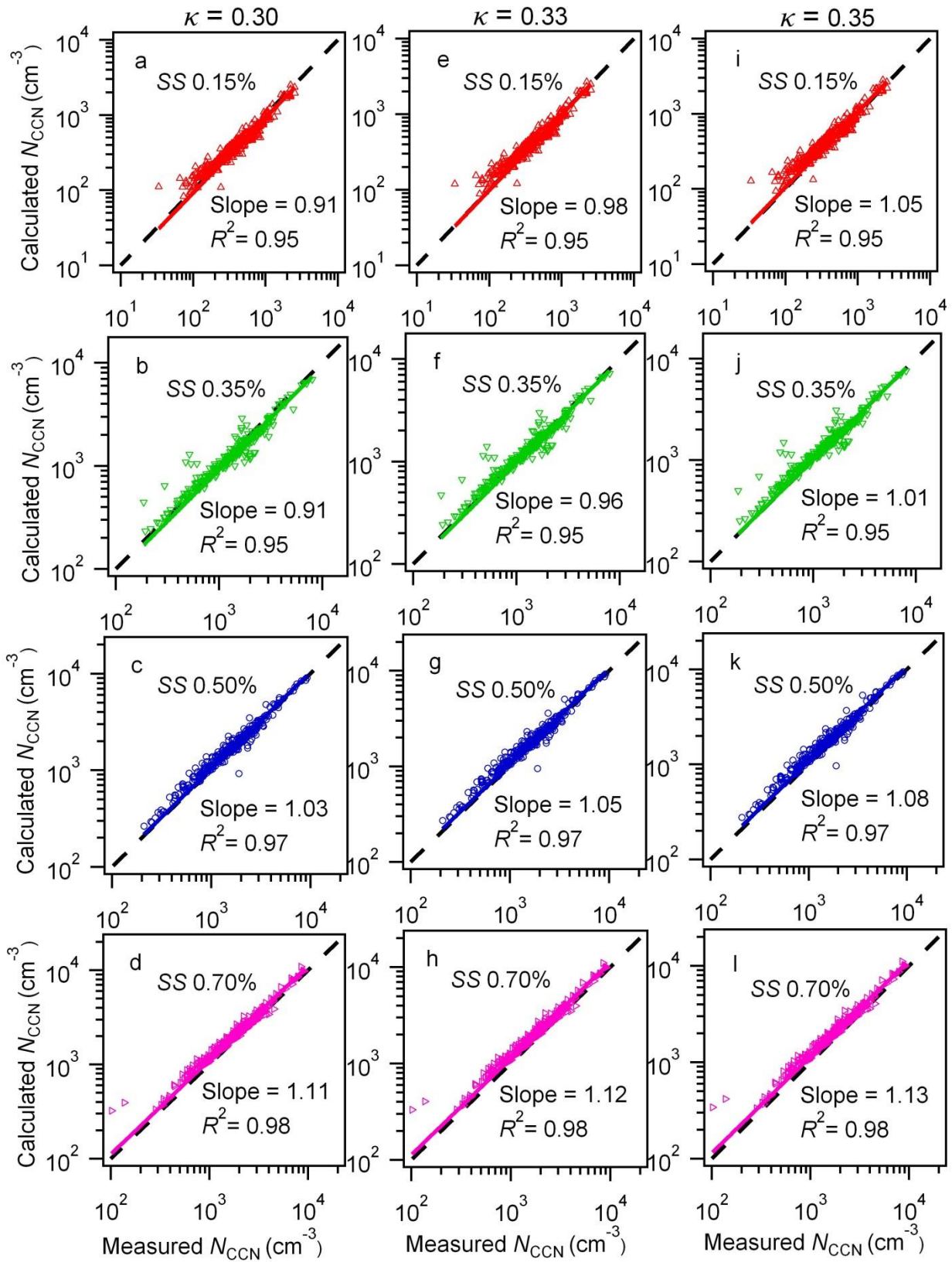


Fig.S2 Correlation of κ_{CCN} derived from CCN measurement and κ_{AMS} from AMS measurement.



105 Fig.S3. Predictions of N_{CCN} based on D_{50} derived from constant κ of (a-d) 0.30, (e-h) 0.33 and (i-
 106 l) 0.35 during whole period, respectively.

107
 108
 109
 110
 111
 112
 113
 114
 115
 116
 117
 118
 119
 120
 121
 122
 123
 124
 125
 126
 127

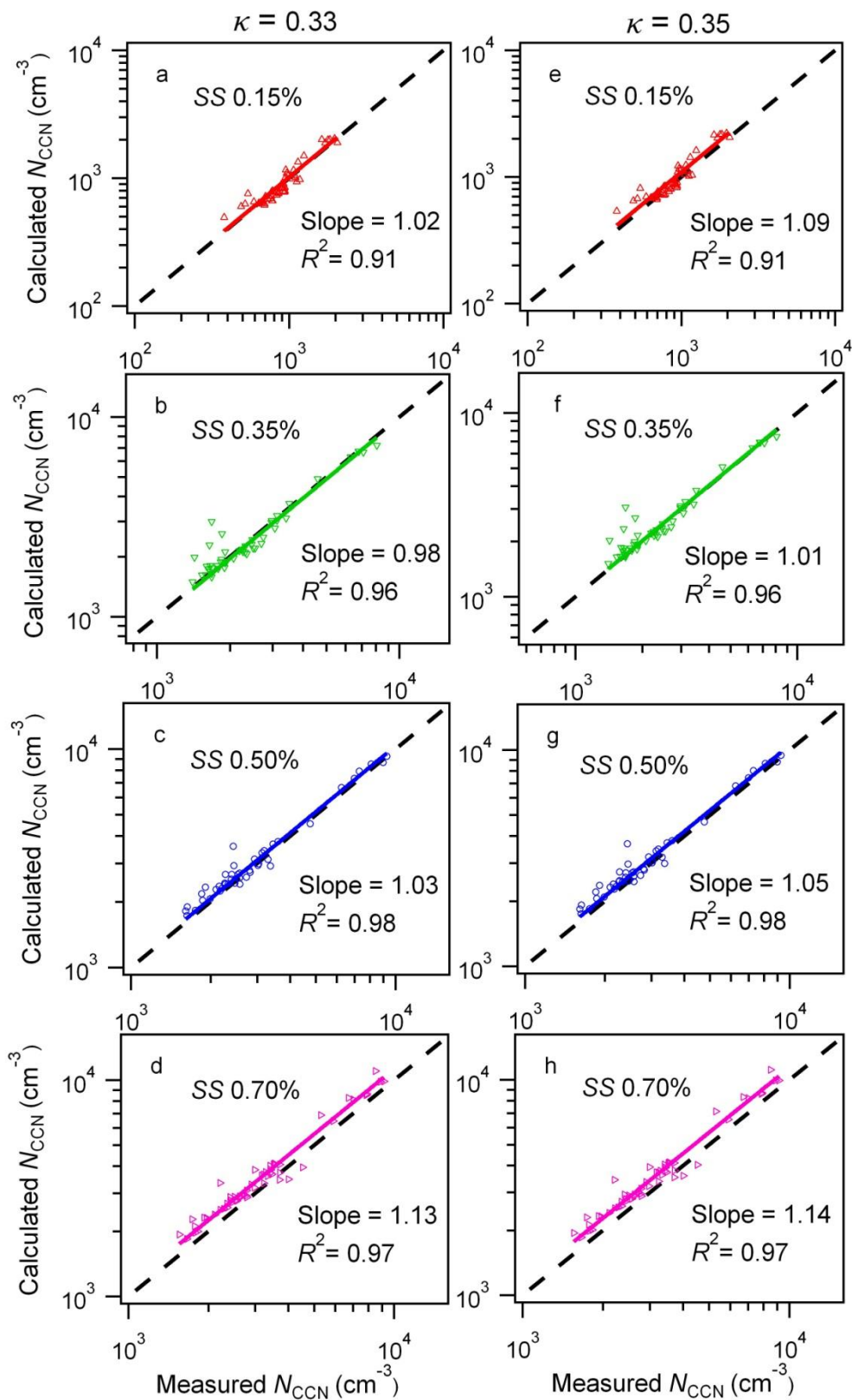
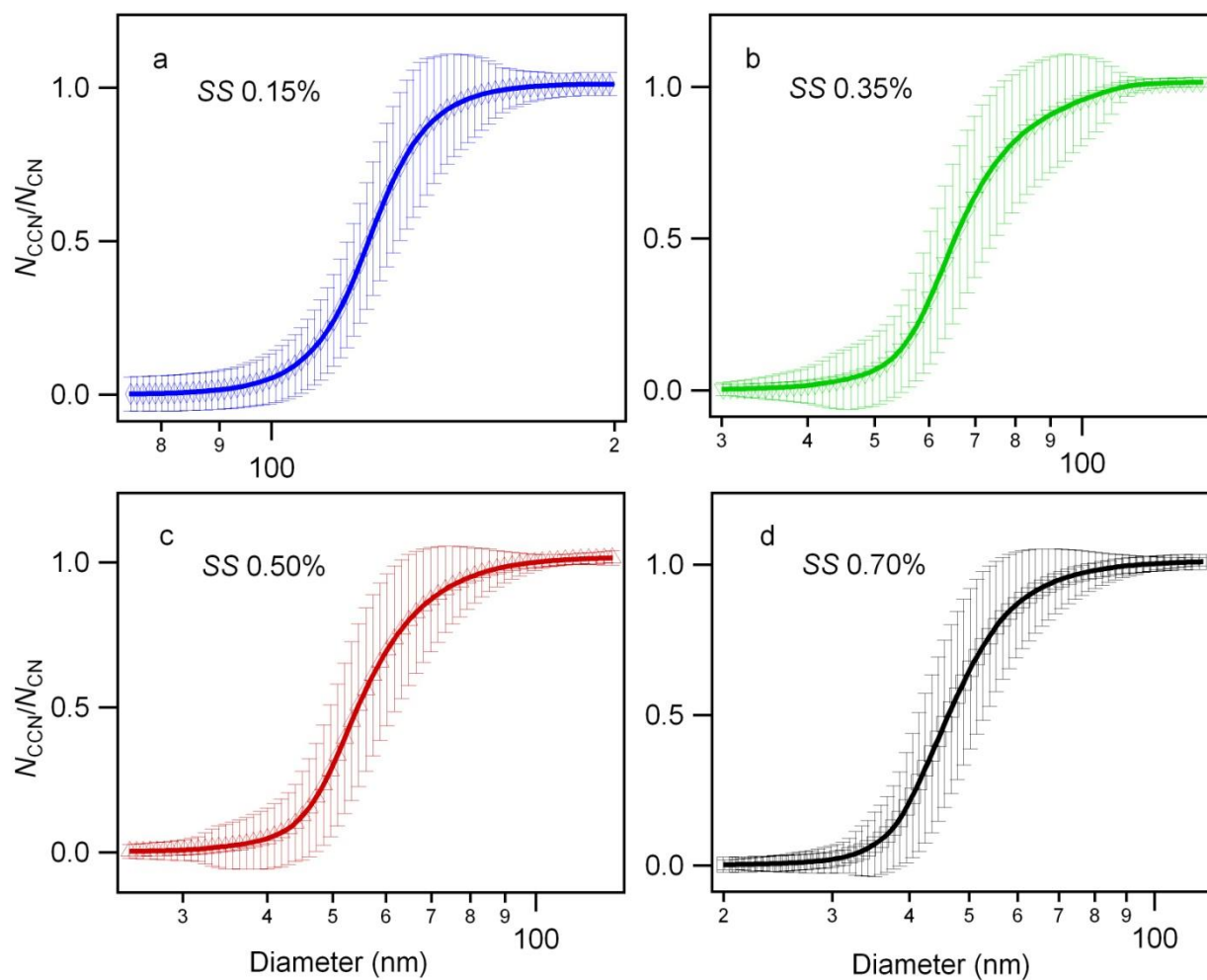


Fig.S4. Predictions of N_{CCN} based on D_{50} derived from constant κ of (a-d) 0.33 and (e-h) 0.35 during hazy period.



128
 129
 130
 131
 132
 133
 134
 135
 136
 137

Fig.S5. The average size-resolved CCN activation ratio at SS (a) 0.15%, (b) 0.35%, (c) 0.50% and (d) 0.70%.

138 **References**

- 139 Bahreini, R., Ervens, B., Middlebrook, A., Warneke, C., de Gouw, J., DeCarlo, P., Jimenez, J.,
140 Brock, C., Neuman, J., and Ryerson, T.: Organic aerosol formation in urban and industrial
141 plumes near Houston and Dallas, Texas, *J. Geophys. Res.*, 114, D00F16,
142 doi:10.1029/2008JD011493, 2009.
- 143 Kuwata, M., Zorn, S. R., and Martin, S. T.: Using elemental ratios to predict the density of
144 organic material composed of carbon, hydrogen, and oxygen, *Environ. Sci. Technol.*, 46, 787-
145 794, 2011.
- 146 Lee, B. P., Li, Y. J., Yu, J. Z., Louie, P. K., and Chan, C. K.: Physical and chemical
147 characterization of ambient aerosol by HR-ToF-AMS at a suburban site in Hong Kong during
148 springtime 2011, *J. Geophys. Res.-Atmos.*, 118, 8625-8639, doi:10.1002/jgrd.50658, 2013.
- 149 Mei, F., Setyan, A., Zhang, Q., and Wang, J.: CCN activity of organic aerosols observed
150 downwind of urban emissions during CARES, *Atmos. Chem. Phys.*, 13, 12155-12169,
151 doi:10.5194/acp-13-12155-2013, 2013.
- 152 Middlebrook, A. M., Bahreini, R., Jimenez, J. L., and Canagaratna, M. R.: Evaluation of
153 composition-dependent collection efficiencies for the Aerodyne aerosol mass spectrometer
154 using field data, *Aerosol Sci. Technol.*, 46, 258-271, 2012.
- 155 Moore, R. H., Raatikainen, T., Langridge, J. M., Bahreini, R., Brock, C. A., Holloway, J. S.,
156 Lack, D. A., Middlebrook, A. M., Perring, A. E., and Schwarz, J. P.: CCN spectra,
157 hygroscopicity, and droplet activation kinetics of secondary organic aerosol resulting from the
158 2010 Deepwater Horizon oil spill, *Environ. Sci. Technol.*, 46, 3093-3100, 2012.
- 159 Roberts, G. and Nenes, A.: A continuous-flow streamwise thermal-gradient CCN chamber for
160 atmospheric measurements, *Aerosol Sci. Technol.*, 39, 206-221, 2005.
- 161 Wang, J., Flagan, R. C., and Seinfeld, J. H.: A differential mobility analyzer (DMA) system for
162 submicron aerosol measurements at ambient relative humidity, *Aerosol Sci. Technol.*, 37, 46-
163 52, 2003.

164

165

166

167

168